Surface relaxation of α-iron and the embedded-atom method

M. I. Haftel, T. D. Andreadis, and J. V. Lill
Code 4651, Naval Research Laboratory, Washington, D.C. 20375-5000

J. M. Eridon*
Code 4672, Naval Research Laboratory, Washington, D.C. 20375-5000
(Received 25 April 1990; revised manuscript received 17 August 1990)

The surface-relaxation properties of bcc iron are calculated with the embedded-atom method (EAM). The main goal of the investigation is to determine what constraints the correct prediction of surface-relaxation quantities places on features of EAM potentials. Seven specific EAM potentials are designed to reproduce experimental bulk properties including elastic constants and phonon frequencies. The features of the embedding function $F(\rho)$ and two-body potential $V(r)$ for each potential are discussed. The perpendicular and parallel surface relaxation quantities for the six faces (100), (110), (111), (210), (310), and (211) are calculated for each potential. The theoretical predictions are compared with the experimental data. Two of the models are found to reproduce the experimental data rather well. The influence of the features of each potential on the atomic spacing is discussed. Our main conclusion is that surface-relaxation predictions can place important constraints on the EAM. In the case of bcc iron, important roles of nearest-neighbor repulsion and second-neighbor attraction are indicated by the experimental surface-relaxation data.

I. INTRODUCTION

The embedded-atom method[1,2] (EAM) has been quite successful in describing the bulk properties of many metals and alloys.[3,4] In this semiempirical model, the total energy of the system is described as the sum of pair potentials between atoms (which includes the shielded Coulomb repulsion between the nuclei), and the sum of embedding energies of individual atoms representing the energy necessary to place the atom in the electron gas produced by the surrounding atoms. In theory this procedure is justified from the local-density approximation of density-functional theory.[5] In practice the pair potential and embedding function, aside from satisfying certain theoretical constraints, are determined by fitting parameters to bulk data.

Surface properties of metals are a logical first testing ground for the robustness of the EAM. One might expect a breakdown of the EAM here because the environment is appreciably different from that of the bulk to which it was fit (e.g., large electron density gradients are present at surfaces). Nevertheless, the convenience of the EAM potentials in molecular-dynamics (MD) simulations and the importance of surfaces in a wide variety of physical phenomena justify the testing of EAM potentials in describing surfaces. This paper performs such a test, in particular for the surface-relaxation properties of bcc iron. Our main goals are first to assess the suitability of the EAM to predict such properties, and second to determine what constraints surface relaxation may place on EAM potentials.

To date, the results are mixed with respect to EAM potential predictions of surface properties. The model, as applied by Daw and Baskes[1-3] and others[4,6] has given surface reconstruction properties of gold[6,7] [for the (100) face] and platinum[8,9] [for the (110) face] in qualitative agreement with experiment.[10,11] However, the EAM predicts too much perpendicular contraction of the relaxed surfaces for Pt(111) and Pt(100) (Ref. 3) compared to experiment, which indicates little relaxation or perhaps a slight expansion.[12] There has not been enough exploration with the EAM to tell whether there are basic shortcomings of the EAM approach for surfaces, or just that there may be shortcomings of particular implementations of the method.

Iron is a good element to test the surface properties of the EAM. Surface-relaxation data are available for six faces,[13-16] and both parallel and perpendicular relaxation occur on three of them.[15] This is in contrast to the data on most other metals where data are usually available only for the low-order faces (100), (110), and (111). Most of the data in these cases generally involve only the perpendicular relaxation of the first two atomic planes, whereas the iron data extend down as far as the fifth atomic plane.

Iron is an interesting element for physical reasons as well. The EAM was originally designed to describe transition metals on the right side of the periodic table, such as Ni, Cu, Au, Pt, Pd, and Ag.[1-4] These are fcc metals with nearly closed d shells in which electronic hybridization can be safely ignored. Iron has more open d shells than these fcc metals, consequently yielding greater electronic hybridization. Iron also has a magnetic interaction, which is also not explicitly accounted for in the EAM formulation. While the magnetic interaction is fairly small, it is enough to account for the differences in stability between different bcc and fcc phases.[17] Given all of the above, it is not obvious that in the case of iron the EAM can be trusted to provide a good model of even bulk material. Nevertheless, as we shall see, a wide

variety of different EAM potentials may be easily derived which reproduce the bulk properties of stable iron, such as lattice constant, sublimation energy, bcc structure, elastic constants, and phonon frequencies. Surface relaxation thus becomes a logical testing ground for the EAM.

This paper examines the surface-relaxation properties of a variety of EAM potentials for iron on faces where experimental data are available.[13-16] Previously, other theoretical approaches, based on simplified force models,[18] and on electrostatics,[19] have yielded fairly good results in describing most of the surface-relaxation properties of iron. Our approach is to use specific EAM potentials to first, test the suitability of the EAM in a surface environment (and that intermediate between surface and bulk), and second, to assess what surface-relaxation data may tell us about the desirability of particular EAM potentials.

In Sec. II of the present paper we describe the particular EAM potentials we consider. Six potentials are generated by a fitting procedure to bulk data described previously by one of us.[20] A seventh potential is generated using a parametrization procedure proposed by Johnson and Oh.[21] The features of the embedding function and two-body potential for each model are discussed. In Sec. III we present the perpendicular and parallel relaxation results for each potential for the (100), (110), (111), (210), (211), and (310) faces compared to the experimental results.[13-16] Several (but not all) of the potentials give surprisingly good agreement with experiment. In Sec. IV we further discuss the features of the two-body potential and embedding function that influence the relaxation of various atomic planes, thus assessing why certain models give good surface-relaxation results in iron. We finally discuss how one, in a very simple fashion, can quickly predict the qualitative features of the surface-relaxation features for any EAM potential in general (including for fcc metals). Section V contains concluding remarks.

II. EMBEDDED-ATOM POTENTIALS

In the embedded-atom model, the total potential energy of the system is considered to be the sum of pair potentials plus the sum of "embedding energies" necessary to place each atom in the electron gas provided by surrounding atoms:[1,2]

$$E=\frac{1}{2}\sum_{i,j\neq i}V(r_{ij})+F(\rho_i)\ , \tag{1a}$$

$$\rho_i=\sum_{j\neq i}\phi(r_{ij})\ , \tag{1b}$$

where $V(r_{ij})$ is the pair potential, $\phi(r_{ij})$ is the electron density produced at site i by a single atom situated at site j, and $F(\rho_i)$ is the embedding function depending only on the total electron density ρ_i at site i.

We fit six EAM potentials following the fitting procedure describing in Ref. 20. The functional forms of V, F, and ϕ are given by

$$V(r)=\sum_{i=-1}^{N}v_i(r/r_c)^i\quad(r<r_c)\ , \tag{2a}$$

$$F(\rho)=f_1(\rho/\rho_e)+\ln(\rho/\rho_e)\sum_{i=2}^{4}f_i(\rho/\rho_e)^{(i-1)}\ , \tag{2b}$$

$$\phi(r)=\phi_s(r_{c1}-r)^\beta\quad(r<r_{c1})\ , \tag{2c}$$

where r_c is the potential cutoff distance [beyond which $V(r)$ is set to zero], ρ_e is the bulk equilibrium electron density, r_{c1} is the atomic electron density cutoff distance (not necessarily the same as r_c), and $\beta\geq 3$ to assure that the electron density fall off goes smoothly to zero at the cutoff. The degree N of the polynomial in Eq. (2a) is 6 if r_e is between the second- and third-neighbor shell, and 8 if it is between the third and fourth. Since the embedding function is expressed as a function of ρ/ρ_e, the scaling factor ϕ_s is arbitrary and has no effect on the evaluation of $F(\rho)$. (This remark is true for pure metals, but the relative scaling of electron density functions does affect the total energy of alloys.[3,22]) The logarithmic form of the embedding function is based on a formulation suggested by Baskes,[23] and satisfies the conditions of zero value and infinite negative slope (if $f_2>0$) at $\rho=0$. The potential coefficients v_i are such that $V(r)$ and $dV(r)/dr$ vanish at $r=r_c$, so $V(r)$ goes smoothly to zero at the cutoff distance. Beyond this, the other v_i are determined by the fit to bulk properties with an additional constraint that $v_{-1}>0$ so that the lattice will be stable under high compression regardless of the coefficients f_i in the embedding function (2b).

The fitting procedure involves matching the first two derivatives of $V(r)$—$V'(r)$ and $V''(r)$—at the near-neighbor distances to values consistent with the measured elastic constants and phonon frequencies, for a given arbitrary electron density function $\phi(r)$. The elastic constants and phonon frequencies are linear functions of these derivatives, so we have N_Q equations for N_D unknowns, where N_Q is the number of elastic constants and phonon frequencies minus one, and N_D is the total number of derivatives of the pair potential. (N_Q is decreased by one because of the existence of the Cauchy relation, which relates C_{12} and C_{44}.) The value of N_D is equal to twice the number of atomic neighbor shells included in the range of the pair potential. The condition for solutions to exist is that $N_D\geq N_Q$, in which case N_D-N_Q of these variables can be explicitly varied while still retaining exactly the same fit to the N_Q physical constants. These free parameters are used to satisfy certain physical constraints, such as stability of the bcc phase over fcc, as well as to allow variation in potential shapes. The actual value of the pair potential (as opposed to its derivatives) is determined by a relation involving the unrelaxed vacancy formation energy. The equilibrium value of the embedding function is determined by the cohesive energy once the pair potential is known. The first derivative of the embedding function is determined by lattice stability (equilibrium stress equals zero). The second derivative of the embedding function is determined by the Cauchy relation, which specifies this value in terms of the two elastic constants C_{12} and C_{44}.

Foiles and Daw[24] have suggested an additional constraint that the potential yields a lattice obeying the

TABLE I. Potential parameters for EAM potentials 1–6 (all units are in eV).

	Potential 1	Potential 2	Potential 3
v_{-1}	10 841.396 17	8521.184 51	1198.756 94
v_0	−130 372.914 81	−99 058.482 61	−11 042.931 09
v_1	690 917.704 70	505 837.922 70	43 252.683 14
v_2	−2 117 762.271 83	−1 489 271.575 74	−93 368.842 92
v_3	4 137 652.351 50	2 786 090.044 20	119 926.019 28
v_4	−5 344 386.737 61	−3 434 830.857 29	−92 621.761 01
v_5	4 564 306.093 10	2 790 970.878 49	38 543.708 15
v_6	−2 485 807.732 33	−1 441 475.792 46	−6887.632 49
v_7	783 542.829 28	429 453.353 40	
v_8	−108 930.718 18	−56 236.675 20	
f_1	−3.237 07	−1.140 47	−1.752 46
f_2	5.876 63	4.591 21	4.835 40
f_3	−5.118 51	−3.547 66	−3.005 78
f_4	1.929 78	1.244 36	0.855 21

	Potential 4	Potential 5	Potential 6
v_{-1}	10 040.289 76	3795.211 46	10 960.088 21
v_0	−124 783.233 01	−33 180.322 60	−131 394.589 65
v_1	682 375.214 93	123 343.146 40	692 662.897 62
v_2	−2 155 779.872 98	−252 775.906 71	−2 108 394.960 63
v_3	4 337 551.540 05	308 479.378 92	4 085 787.571 96
v_4	−5 766 362.923 48	−224 208.762 19	−5 230 260.288 79
v_5	5 067 116.723 75	89 882.737 85	4 425 451.146 94
v_6	−2 839 389.356 78	−15 335.483 12	−2 388 178.983 71
v_7	921 078.525 60		746 353.045 69
v_8	−131 846.907 83		−102 985.957 64
f_1	−1.697 76	−1.747 44	−1.732 34
f_2	4.886 50	5.046 10	4.923 20
f_3	−3.091 08	−3.427 22	−3.164 50
f_4	0.887 48	1.065 93	0.924 20

TABLE II. Physical bulk parameters of the EAM potentials. E_{v1}^F is the relaxed vacancy formation energy. Only the values of the frequencies of phonon modes exactly fit to experiment are indicated. α is the thermal-expansion coefficient at 300 K and zero external pressure. The experimental value of α (at 298 K, ambient pressure) is 12×10^{-6}/K.

	Potential 1	2	3	4	5	6	JO
E_c (eV)	4.28	4.28	4.28	4.28	4.28	4.28	4.29
a (Å)	2.8665	2.8665	2.8665	2.8665	2.8665	2.8665	2.86645
E_{v1}^F (eV)	1.59	2.00	1.42	1.41	1.59	1.48	1.57
C_{11} (Mbar)	2.331	2.331	2.331	2.331	2.331	2.331	2.295
C_{12} (Mbar)	1.354	1.354	1.354	1.354	1.354	1.354	1.354
C_{44} (Mbar)	1.178	1.178	1.178	1.178	1.178	1.178	1.167
ΔE (eV)	0.096	0.038	0.034	0.023	0.142	0.082	0.028
$\Delta\mathcal{V}$ (%)	22.2	−10.8	+6.3	+2.4	−6.9	−5.3	+6.5
r_c (Å)	4.6	4.6	3.9	4.6	3.9	4.6	3.48
r_{c1} (Å)	3.5	3.5	3.9	3.5	3.9	3.9	3.48
β	3	3	6	6	6	6	6
α (10^{-6}/K)	75.8	30.7	9.7	12.6	25.0	20.2	8.4
				Phonon frequencies			
(100) L (THz)	8.56	8.56		8.56		8.56	
(0.5,0.5,0)$T1$ (THz)				4.47		4.47	
(0.5,0.5,0.5)L (THz)	7.21	7.21					

universal equation of state proposed by Rose *et al.*[25] and in so doing guarantee a satisfactory value for the thermal-expansion coefficient. We have not applied this constraint but we have estimated the thermal-expansion coefficient for each potential. (See the later discussion of Table II).

We have constructed a set of six EAM potentials (hereafter labeled as potentials 1–6). The coefficients v_i and f_i [Eqs. (2a) and (2b)] appear in Table I. All have been fit to the same cohesive energy (4.28 eV/atom), lattice constant (2.8665 Å), and elastic constants as determined by experiment ($C_{11}=2.331$ Mb, $C_{12}=1.3544$ Mb, $C_{44}=1.1783$ Mb).[26] In addition some of the potentials are explicitly fit to certain phonon frequencies[27] (see Table II). All of these potentials yield lattices that are stable under high compression (i.e., $v_{-1}>0$) and under bcc→fcc transformation. Also, all but one predict an unrelaxed vacancy formation energy of 1.6 eV (potential 2 has $E_{v1}^{\rm UF}=2.0$ eV), with this value decreasing by various amounts upon relaxation of the lattice (see Table II). All potentials fit to phonon frequencies have potential cutoffs between the third- and fourth-neighbor shells, while those not so fit have cutoffs between the second- and third-neighbor shells. For all potentials the number of included neighbor shells is the minimum such that $N_D>N_Q$; in fact, for all potentials $N_D-N_Q=2$, and V'' at the last two included neighbor shells are used as free parameters to (1) demand bcc stability, and (2) vary the potential shapes. All electron density cutoffs are between the second- and third-neighbor shells.

We also consider a seventh EAM potential following the procedure proposed by Johnson and Oh (we label this potential JO). We refer the reader to their paper[21] for details. Here the potential $V(r)$ is a cubic polynomial until a matching point between the second- and third-neighbor shells whereupon the potential assumes a different cubic form continuous and continuously differentiable at the matching point, and having zero value and slope at the cutoff radius (before the third-neighbor shell). The matching and cutoff radii satisfy

$$r_i=r_2+k_i(r_3-r_2)\ , \tag{3}$$

where i is either m (for matching) or c (for cutoff), and r_2 and r_3 are the second- and third-neighbor distances, respectively. In addition, the potential is "stiffened"[21] inside the first-neighbor shell to be in compliance with the equation of state of Rose *et al.*[25] The embedding function has the form

$$F(\rho)=F_0\{[n/(n-m)(\rho/\rho_e)^m-[m/(n-m)](\rho/\rho_e)^n]\}, \tag{4a}$$

with the atomic electron density

$$\phi(r)=\phi_s(r_1/r)^\beta\ , \tag{4b}$$

where ρ_e is the bulk equilibrium electron density at a lattice site, and r_1 is the nearest-neighbor distance in the equilibrium bulk. The integers n,m satisfy

$$nm\beta^2=(9a^3/2)(C_{12}-C_{44})/(E_C-E_{v1}^{\rm UF})\ . \tag{5}$$

A cutoff is applied to $\phi(r)$ similarly as to $V(r)$.

The physical parameters for all potentials appear in Table II. The lattice constant (2.866 45Å) and cohesive energy (4.29 eV) used in potential JO are taken from Ref. 21 and differ very slightly from those used in our other potentials. Also, the unrelaxed vacancy formation energy is somewhat different (1.75 eV).[28] We have confirmed, by considering an alternate JO potential fit to the same physical constants as potentials 3 and 5, that these differences have an insignificant effect on bulk phonon frequencies or surface-relaxation predictions (i.e., at the $<1\%$ level). In parametrizing the cutoffs, we take $k_m=0.1$, $k_c=0.5$ for both $V(r)$ and $\phi(r)$, which leads to a cutoff of 3.46 Å. The embedding function power parameter n is taken to be $\sqrt{1/8}$, and the electron density parameter $\beta=6$.[21]

Table II also gives other physical bulk properties for each potential. ΔE is the increase in energy for fcc structure over that in bcc. $\Delta\mathcal{V}$ is the percent increase in atomic volume of the metastable fcc phase compared to that of bcc. The last row indicates the phonon frequency modes explicitly fit to experimental measurements.[27] Since all potentials are fit to the same elastic constants, they all give good phonon dispersion results at low q, but there is no guarantee that they will further fit the experimental frequencies except for the particular modes indicated in Table II. The thermal-expansion coefficient was estimated by computing the average stress on the lattice for temperatures near 300 K and searching for the lattice constant that yields zero average stress for each temperature. This method is only approximate due to the fluctuations over the time steps used in the molecular-dynamics simulation, and our accuracy is about 10%. This accuracy is adequate to distinguish our potentials as α varies very widely between different models. (The experimental value is 12×10^{-6}/K.)

We group the potentials considered into three classes according to the phonon modes fit (if any). The first class (potentials 1 and 2) includes those fit to the (100) longitudinal and $(\frac{1}{2}\frac{1}{2}\frac{1}{2})$ longitudinal modes. The second class (4 and 6) were fit to the (100) longitudinal and $(\frac{1}{2}\frac{1}{2}0)$ transverse-1 modes. The third class (3, 5, and JO) were not explicitly fit to any phonon dispersion data. As mentioned previously, within each class two of the V'' quantities were explicitly varied to allow for bcc stability and to vary the potential shapes.

Figures 1–3 display the bulk phonon dispersion curves for each potential for the $q00$, $qq0$, and qqq modes, respectively. All potentials give reasonably good fits to the data. Potentials 1 and 2 fall somewhat below the data for the $qq0$ transverse modes near the zone boundary, and also suffer too large a "dip" in the qq longitudinal mode near $q/q_0=0.7$. This happens despite these potentials being fit to the qqq (longitudinal) frequency at the zone boundary. Potential 6 gives an excellent fit overall to all frequencies, and potentials 4 and 5 also give quite good fits. Potentials 3 and JO also give satisfactory fits despite the fact that the phonon dispersion data were not used in the construction of these potentials. It is instructive here to note that requiring an *exact* fit to certain points on the dispersion curves does not necessarily guarantee the best fit overall.

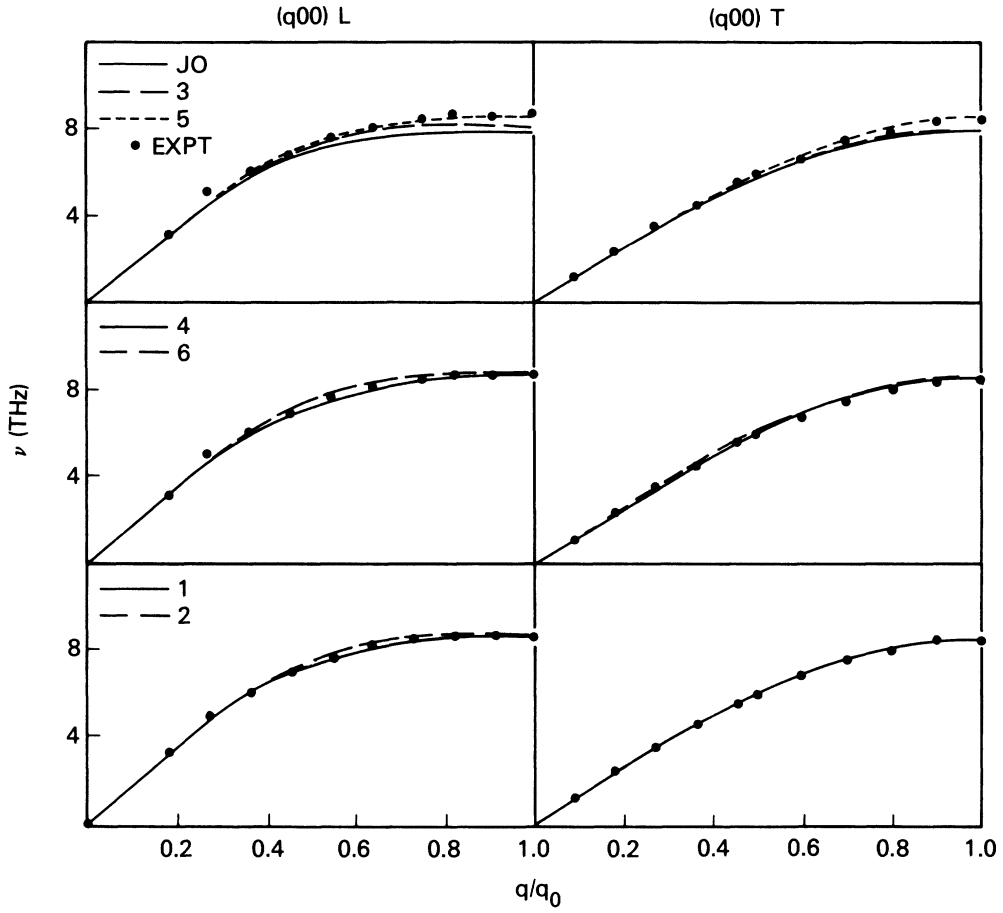

FIG. 1. Phonon frequencies for (q00) longitudinal and transverse modes. For all phonon frequency plots $q_0 = 2.192$ Å.

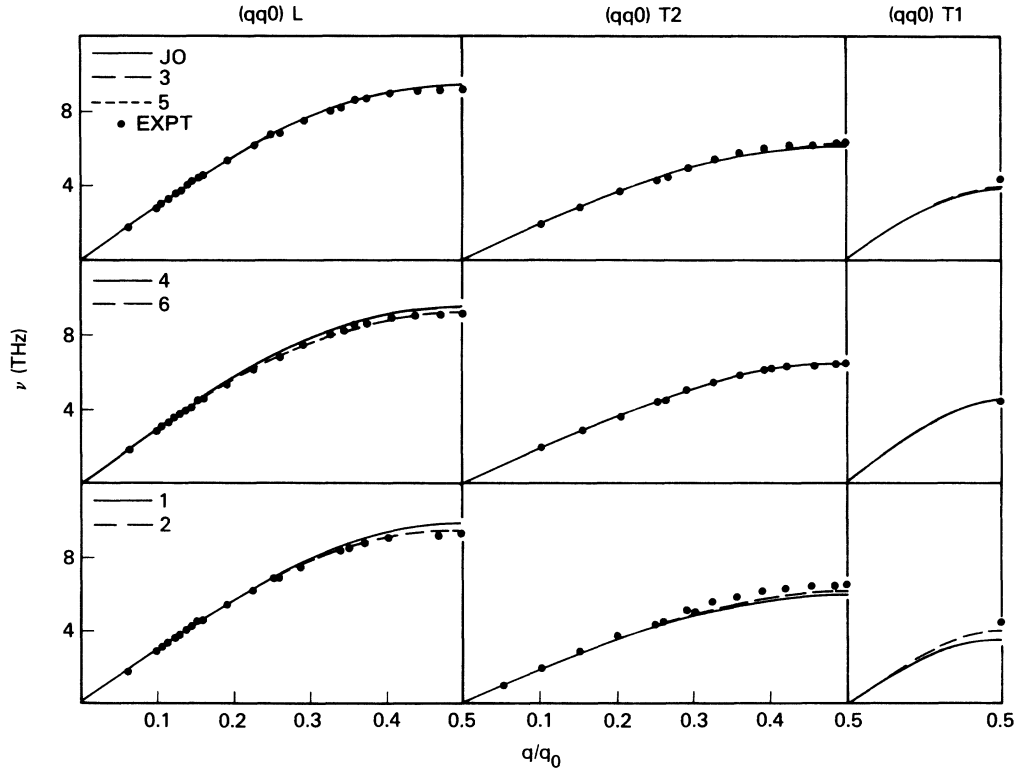

FIG. 2. Phonon frequencies for (qq0) longitudinal and transverse (1 and 2) modes.

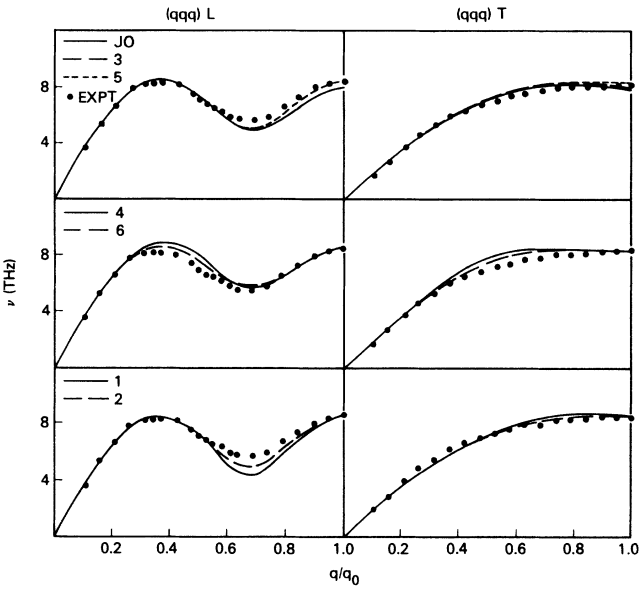

FIG. 3. Phonon frequencies for (*qqq*) longitudinal and transverse modes.

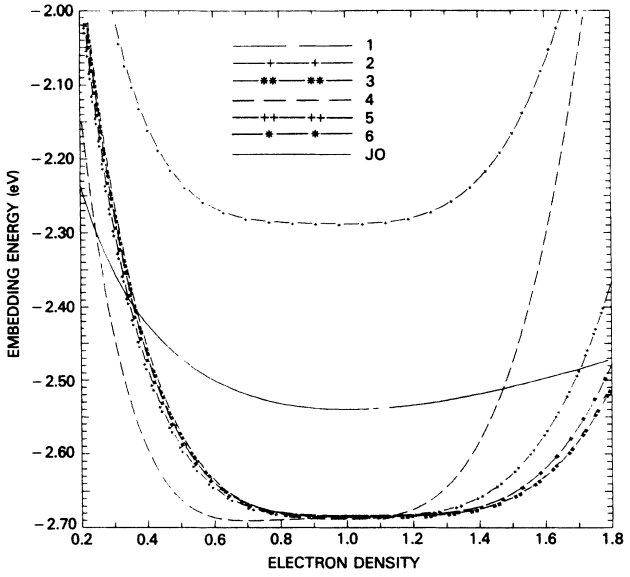

FIG. 5. Embedding function $F(\rho)$ for each EAM model. $\rho=1$ corresponds to the bulk equilibrium electron density at a bcc lattice site.

Figure 4 illustrates $V(r)$ for the potentials, Fig. 5 the embedding functions, and Fig. 6 the atomic electron densities $\phi(r)$. In plotting these quantities we have adopted Johnson and Oh's convention[21] and modified the functions defined in Eqs. (2) by adding a multiple of ρ to the embedding function, and subtracting twice the atomic electron density $\phi(r)$ from the two-body potential such that the embedding function has a minimum at the bulk equilibrium electron density. This transformation leaves the total potential energy of any atomic configuration invariant, and facilitates assessing the roles of various features of the EAM in surface calculations as well as carrying out comparisons of different EAM interactions. [Of course, neither the $V(r)$ defined by Eq. (2) nor the "modified" $V(r)$ plotted in Fig. 4 is nature's true $V(r)$, i.e., the potential between an isolated two-atom cluster.]

Examining first the $V(r)$ curves (Fig. 4), we see that the potential shapes vary considerably. While, strictly speaking, we know that the bulk data do not uniquely determine the potential shape, still the variation is surprising.

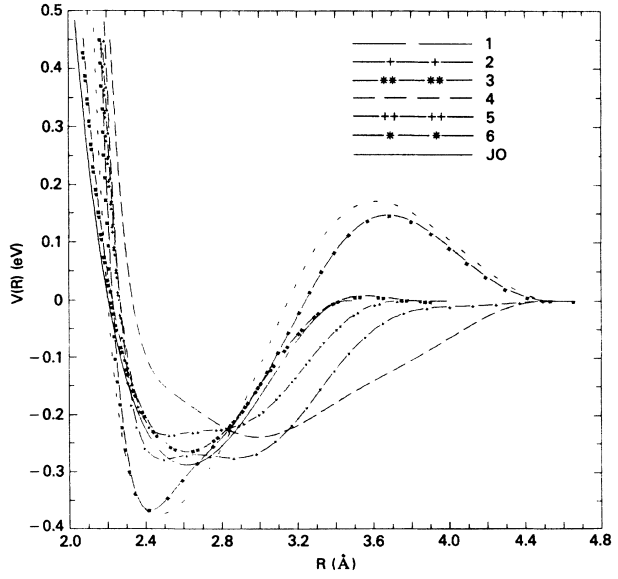

FIG. 4. Two-body potential $V(r)$ for each EAM model. Potentials 1–6 are labeled by their numbers, and JO is labeled by *JO*.

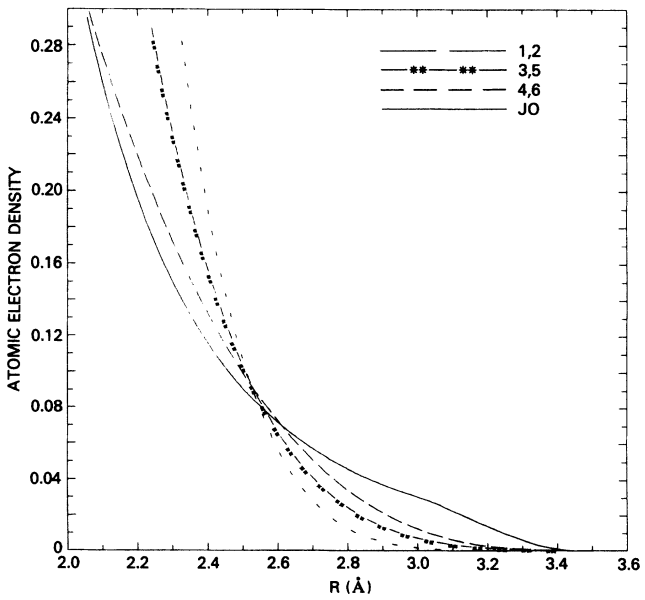

FIG. 6. Atomic electron density $\phi(r)$ for each EAM model.

All are repulsive ($dV/dr<0$) for $r<2.2$ Å, but some (3,4,JO) have a good deal of curvature, like a Morse potential, while others are fairly flat (1,2,5). As we shall see, surface-relaxation properties are mainly influenced by the slope of the potential at the first- and second-nearest-neighbor distances (2.48 and 2.87 Å, respectively). Potential 1 is unique in that it is still repulsive at the second-nearest-neighbor distance with a minimum near $r=3.0$ Å. Also, although not readily apparent in Fig. 5, $F(\rho)$ for potential 1 has an additional minimum near $\rho\approx 0.7$ about 0.01 eV lower than at the bcc bulk equilibrium electron density ($\rho=1$). In the course of our calculations we discovered, with this potential, a bulk phase of lower cohesive energy (4.29 eV) than the cubic bcc phase, characterized by lattice sites on a given 211 plane the same as the bcc sites, but with the interplanar distance stretched by 20%. We do not know if this is the most stable phase, but this does indicate a pathology of potential 1. It seems likely that the behavior of the minima of $V(r)$ and $F(\rho)$ accounts for this spurious phase. Additionally, the tendency for the lattice to expand with this potential may be connected with its unrealistically large thermal-expansion coefficient (see Table II). Moreover, our calculations of the next section will show that surface-relaxation quantities are sensitive to different potential shapes not distinguished by the bulk properties, and that these surface quantities can be used to help fix the potential shape.

The embedding functions (Fig. 5), "normalized" as described above, have fairly similar features. (This is partly by construction.) All models are rather flat between $\rho=0.7$ and 1.4, where $\rho=1$ is defined to be the bulk equilibrium electron density. The steepness of $F(\rho)$ does vary considerably at very small and very large ρ. The very small and very large ρ behavior is not probed in surface-relaxation calculations, but the region $0.5\leq\rho\leq 1.3$ does affect surface predictions. In this range potentials 1–6 behave fairly similarly, but JO is rather less steeply varying at the limits of this region. While the embedding functions of different models are more similar to each other than $V(r)$, differences do exist. Furthermore, we shall see that the embedding functions play a very important role in contracting the spacing of the first two atomic layers in surface relaxation.

We finally note the fcc-bcc properties of the different EAM interactions. The $\Delta\mathcal{V}$ properties are of special interest because, as we shall see, the models with $\Delta\mathcal{V}>0$ generally give better surface-relaxation results. The potentials with $\Delta\mathcal{V}>0$ (1,3,4,JO) generally have the minimum in $V(r)$ beyond the nearest-neighbor distance (2.48 Å). This means that the nearest-neighbor two-body force is repulsive in the equilibrium bulk. The results of the next section will indicate that this feature is desirable to explain the surface-relaxation data.

III. SURFACE-RELAXATION CALCULATIONS

We utilize a molecular-dynamics program written by us (DAMSEL) to find the minimum energy configuration of the relaxed lattice. This program employs a link-cell algorithm[29] to generate neighbor lists for the purpose of computing forces on atoms and total energy. In surface calculations periodic boundary conditions are employed in two orthogonal directions in the plane as appropriate for the exposed plane under consideration. No periodic boundary conditions are applied in the z direction perpendicular to the plane, but a bottom layer of cells, of depth comparable to but larger than the cutoff distance, is frozen in bulk equilibrium positions to simulate the underlying bulk and to stabilize the lattice. Starting from a terminated bulk configuration, we search for the configuration with a local total potential energy minimum by employing the conjugate gradient method.[30] The number of (active) atoms, the surface unit-cell structure, and the number of layers of atoms used in each surface calculation are listed in Table III. Doubling the number of (active) layers has a negligible effect ($<0.1\%$) on surface-relaxation distances, but changes surface energies at about the 2–3 % level.

Table IV lists the relaxation distances and surface energy for each potential for each surface. The usual notation is employed: d_{ij} is the perpendicular distance between planes i and j; a_{ij} is the registry distance between planes i and j (see Refs. 15) under relaxation. The registry shift is the difference between a_{ij} and its terminated bulk value, and this shift indicates the relative lateral shifting of the two planes. For the (211) face with potential 1, the lattice relaxes to a structure with an underlying bulk configuration which is not bcc (see preceding discussion in Sec. II). For this reason we omit surface-relaxation results for potential 1 for (211). Figures 7–9 illustrate the surface-relaxation results, and the experimental measurements,[13–16] in a way so that trends among various potentials and for different surfaces can be more easily seen.

The main features from Table IV and Figs. 7–9 are as follows: Most potentials predict the correct trend vis á vis the corresponding distances in the bulk; i.e., expansion or contraction from the terminated bulk distances is usually in agreement with experiment. The contraction of the first two planes, which is quite large experimentally, is underestimated by almost all of the potentials for all of the surfaces. Potentials with positive $\Delta\mathcal{V}$ give the best results, whereas potentials with negative $\Delta\mathcal{V}$ "under relax," i.e., the d_{ij} and the a_{ij} are usually too close to the terminated bulk values. Overall, potentials 3 and JO give the best agreement. However, even with these potentials, occasionally large disagreements with experiment do

TABLE III. Configurations of atoms used in surface-relaxation calculations with the conjugate gradient method.

Surface	Active atoms	Unit cells $x\times y$	Active layers
(100)	225	5×5	9
(110)	240	5×4	12
(111)	312	3×4	26
(210)	225	3×5	15
(211)	288	4×6	12
(310)	320	2×5	32

occur, e.g., d_{12} (111) for JO and d_{23} (210) for potential 3. Potential 1 also gives good results, except for (211), but this potential predicts an anomalous bulk phase. Potential 4, which has a positive $\Delta\mathcal{V}$, gives fairly good results for d_{ij}, except it does tend to "under relax," but fails to predict the parallel relaxations a_{ij}.

IV. DISCUSSION

To better understand the surface-relaxation results, we will first consider the expected influences $V(r)$ and $F(\rho)$ each might separately have on the d_{ij} and the a_{ij}. The main features of $V(r)$ that affect surface relaxation are the slope of the potential at the first- and second-nearest-neighbor distances. (In all of the following discussion references to the first- or second-neighbor distances will mean the corresponding distances in the equilibrium bulk. Also, forces on atomic planes will refer to those felt in the initial terminated bulk configuration, unless otherwise noted.) The slope of the potential determines the force felt by an atom from another, and forces near or at the surface will be lacking the forces that would have been exerted in the bulk by the missing neighbors. Nearest-neighbor atoms exert a repulsive (attractive) force if the slope of the potential is negative (positive) at this point. So atoms near the surface missing nearest-neighbor atoms will experience an upward (downward) force from the absence of these atoms. The same is true for missing second neighbors. The interplanar spacing will mainly depend on the relative total of such "forces" on each plane, which in turn depends on the configuration of missing neighbors for each plane. Of course, the type of relaxation properties described has to be superimposed on the relaxation properties dictated by the embedding function.

Taken by itself, the embedding function along would produce a pattern of alternating contraction and expansion of interplanar distances. Atoms on the top plane of the terminated bulk experience a much lower electron density than the rest of the system. To try to minimize $F(\rho)$ the planes will tend to arrange themselves such that $\rho=1$ for the top layer. This normally means a large con-

TABLE IV. Surface-relaxation quantities. The d_{ij} and a_{ij} are in angstroms. The surface energy E_s is in eV/Å^2.

		Potential						
Surface	Experiment	1	2	3	4	5	6	JO
(100)								
E_s		0.0902	0.1094	0.0936	0.0768	0.0897	0.0760	0.0971
d_{12}	1.41±0.04	1.472	1.397	1.388	1.343	1.372	1.332	1.486
(110)								
E_s		0.0912	0.1008	0.0794	0.0533	0.0794	0.0572	0.0878
d_{12}	2.04±0.04	2.076	2.022	2.006	1.970	2.002	1.974	2.014
(111)								
E_s		0.1025	0.1238	0.1086	0.0826	0.0997	0.0858	0.1082
d_{12}	0.70±0.03	0.791	0.766	0.766	0.779	0.744	0.759	0.846
d_{23}	0.75	0.893	0.826	0.743	0.704	0.814	0.749	0.710
d_{34}	0.86	0.862	0.847	0.882	0.869	0.857	0.861	0.889
d_{45}	0.81	0.785	0.813	0.824	0.849	0.812	0.837	0.832
(210)								
E_s		0.0974	0.1126	0.0899	0.0679	0.0903	0.0701	0.0967
d_{12}	0.50±0.03	0.577	0.593	0.543	0.561	0.569	0.578	0.602
d_{23}	0.57±0.03	0.584	0.632	0.798	0.623	0.824	0.634	0.612
d_{34}	0.75±0.03	0.798	0.655	0.739	0.667	0.667	0.616	0.754
d_{45}	0.61±0.03	0.583	0.629	0.578	0.601	0.623	0.630	0.566
a_{12}	2.06±0.03	2.028	1.909	1.961	1.904	1.903	1.870	2.004
a_{23}	1.95±0.05	1.993	1.926	2.002	1.996	1.936	1.929	2.008
a_{34}	1.92±0.05	1.880	1.916	1.917	1.928	1.930	1.928	1.925
a_{45}	2.00±0.05	1.923	1.926	1.933	1.935	1.924	1.932	1.923
(310)								
E_s		0.0968	0.1147	0.0926	0.0722	0.0925	0.0731	0.0985
d_{12}	0.76±0.03	0.801	0.849	0.770	0.800	0.815	0.829	0.800
d_{23}	1.02±0.03	1.037	0.919	0.995	0.935	0.931	0.886	0.935
d_{34}	0.87±0.04	0.859	0.894	0.838	0.863	0.885	0.893	0.863
a_{12}	1.94±0.05	1.943	1.811	1.899	1.823	1.811	1.873	1.940
a_{23}	1.84±0.05	1.766	1.804	1.837	1.848	1.805	1.830	1.816
(211)								
E_s			0.1165	0.0898	0.0645	0.0929	0.0712	0.0992
d_{12}	1.05±0.03		1.141	1.087	1.070	1.112	1.165	1.122
d_{23}	1.23±0.03		1.178	1.203	1.184	1.187	1.191	1.198
a_{12}	1.41±0.03		1.654	1.488	1.452	1.622	1.520	1.468
a_{23}	1.69±0.03		1.662	1.743	1.651	1.678	1.740	1.774

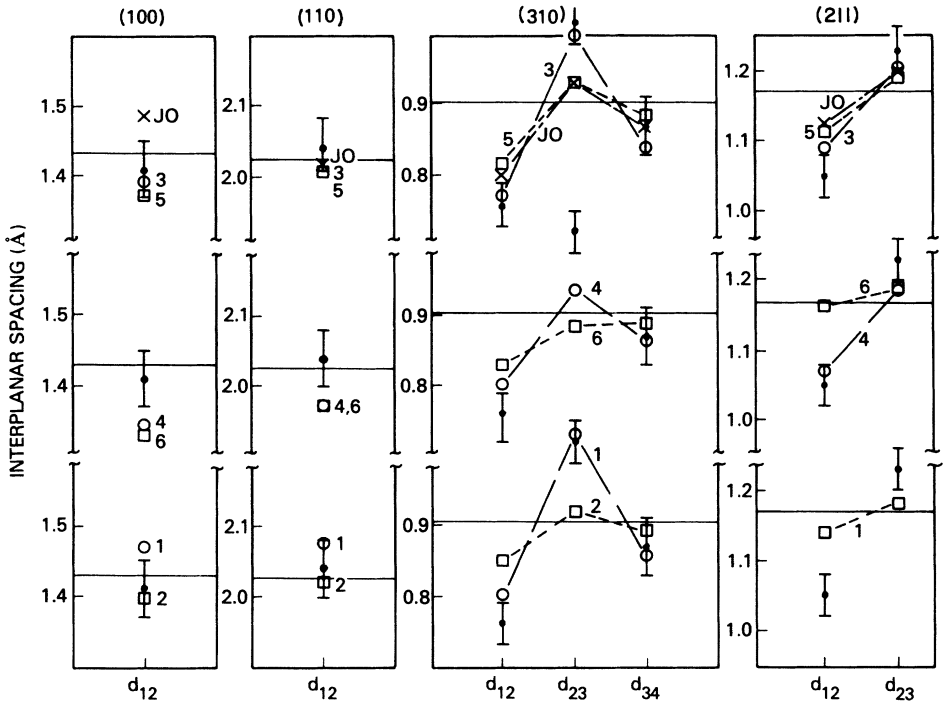

FIG. 7. Interplanar spacing d_{ij} for the (100), (110), (310), and (211) faces. The open circles, open squares, and X's show the calculated values for each EAM model for the d_{ij} indicated along the abscissa and face indicated at the top. The dashed lines connect the calculated points for each model to guide the eye. The horizontal solid line indicates the (constant) terminated bulk value for d_{ij}. The black dots, with error bars, are experimental values from Refs. 13–16.

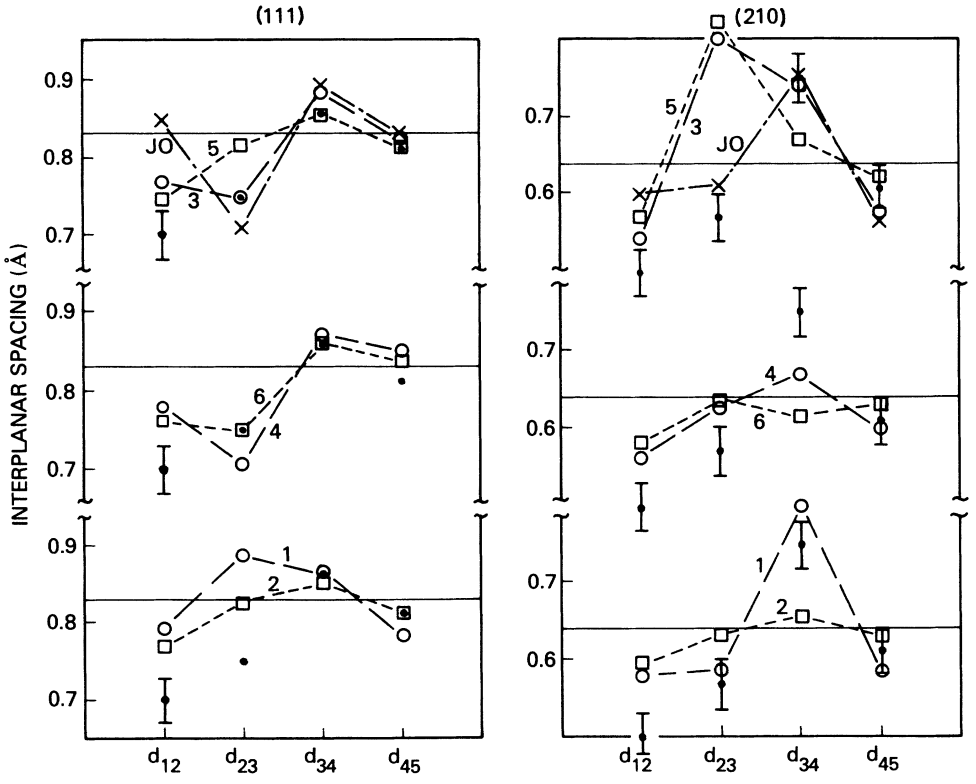

FIG. 8. Interplanar spacings d_{ij} for the (111) and (210) faces. The interpretation of the plot is the same as Fig. 7.

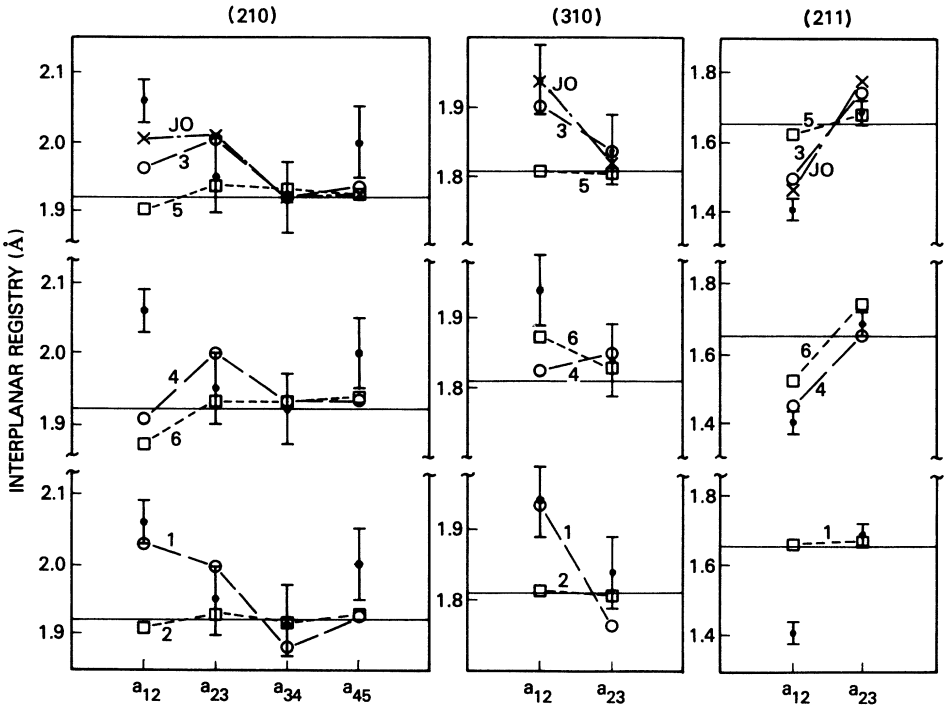

FIG. 9. Registry distances a_{ij} for the (210), (310), and (211) faces. The interpretation of the plot is the same as Fig. 7.

traction in d_{12}. But now the second layer will have a $\rho=1$ contribution just from the electrons in orbitals belonging to the atoms from above. Again to achieve a total $\rho=1$, the second interplanar distance d_{23} will have to greatly expand. This pattern would continue forever, forming a "sawtooth" pattern of interplanar distances. The presence of the two-body force prevents this from happening. Nevertheless, it is clear that the top layer of atoms will experience a strong downward force since the force from the embedding function is $-(dF/d\rho)\nabla\rho$, and $dF/d\rho$ is normally negative for $\rho<1.0$, and also the electron density gradient at the surface points strongly into the metal.

The interplanar spacings d_{ij} of various surfaces, therefore, display the competing influences of the missing neighbor two-body forces, and a possible alternating contraction-expansion pattern that would ensue from a pure embedding function picture. Table V gives the number of missing first and second neighbors for each surface for planes going progressively deeper into the solid. It is evident from the table that surface relaxation tests many different combinations of first- and second-neighbor forces. (We have simplified the true picture somewhat; surface relaxation does probe the potentials at distances other than bulk near-neighbor distances since interatomic spacings change when the lattice relaxes.) The lower coordination faces [like (111), (310), and (210)] test the EAM in situations markedly different than the bulk—both with respect to neighboring atom forces and electron densities. Also, since many different combinations of forces are tested and a wide range of models are considered, we can begin to address the question of not only the quality of particular EAM interactions, but also the validity of the EAM in general for surface properties.

Many of the experimental trends are explainable in terms of the EAM. The strong effect of the contraction of the distance d_{12} between the first two planes due to decreased electron density at the surface is readily apparent. The particular models usually predict this feature qualitatively, but underestimate it. The "sawtooth" pattern ($d_{12}<d_{23}>d_{34}<d_{45}$, etc.) dictated by electron density properties shows up quite strongly for

TABLE V. Missing first- and second-nearest neighbors.

	Face (110)		(211)		(100)		(111)		(310)		(210)	
Plane	1st	2nd	1st	2nd	1st	2nd	1st	2nd	1st	2nd	1st	2nd
1	2	2	3	3	4	1	4	3	4	2	4	2
2	0	0	1	1	0	1	1	3	2	1	2	2
3	0	0	0	0	0	0	1	0	0	1	2	1
4	0	0	0	0	0	0	0	0	0	0	0	1

the (310) and (211) faces, both experimentally and for most EAM potentials. This pattern is much subdued for the (111) and (210) faces both experimentally and theoretically. In fact, a large increase for d_{34} (instead of d_{23}) is measured for the (210) face, which is predicted by several EAM potentials.

While none of the EAM interactions gives a detailed fit to every data point, the potentials with the Morse-like shapes (3,4,JO) fare rather well. (These are also the only potentials with reasonable thermal-expansion coefficients). Except for d_{12} on (111), JO gives good fits for all of the other data points including the parallel relaxation data (a_{ij}). Potential 3 falters on d_{23} for (210), but otherwise does well. Potential 4 gives qualitatively correct trends, but significantly underestimates d_{ij} when d_{ij} is greater than the bulk value. Its predictions for a_{ij} on (210) and (310) are also well below the data. Discrepancies, when they occur for these potentials, are for the faces with the most missing neighbors (see Table V), which is where the EAM would be most severely tested.

Most of the surface-relaxation EAM results are consequences of the shape of $V(r)$ along with the strong decrease in d_{12} associated with the large electron density gradient. Potential 2, for example, with its very flat shape, generally gives results close to terminated bulk because of the smallness of the missing first- and second-neighbor forces. Potentials 4 and 6 suffer to a lesser degree the same fate thanks to the flatness of the potential at the nearest-neighbor distance. Potential 1, with its emphasis on nearest-neighbor repulsion, gives good surface-relaxation results [except for (211)]. This potential, although it must be considered unphysical, is still useful for considering the influence of its features on d_{ij}, and a_{ij} on faces other than (211). The calculated surface-relaxation quantities for these faces, however, represent those of a metastable phase with underlying bulk bcc structure. In the surface calculation for the (211) face, the initial terminated bulk with cubic bcc structure naturally relaxes, in the conjugate gradient algorithm, to a structure with the underlying "stretched" bcc structure described in Sec. II.

A careful examination of Table V and the potential curves themselves is useful in assessing the EAM and the differences between various models for different faces. For example, potential JO has approximately the same amount of nearest-neighbor repulsion as second-nearest-neighbor attraction. In terms of forces on (unrelaxed) atom planes, missing nearest neighbors will lead to net upward forces, and missing second neighbors to downward forces. With reference to Table V, the forces on the first three (111) planes should be up, strongly down, and up, respectively. This should lead to a very large d_{12}, a very small d_{23}, and large d_{34}. This does occur, except d_{12} is only slightly larger than the bulk value. A large counterbalancing decrease in d_{12} occurs due to the large downward force on the top plane produced by the embedding function $F(\rho)$.

It is interesting that potential 3, whose $V(r)$ is similar to JO, gives a significantly smaller d_{12} on (111) (and a slightly larger d_{23}). This occurs because the embedding function for potential 3 is steeper around the "edges" (i.e., at $\rho \approx 0.5$ and $\rho \gtrsim 1.4$) than JO, leading to a more pronounced increase of d_{23} over d_{12}, canceling out much of the opposite effect coming from the two-body potential function. This influence of $F(\rho)$ shows up also on the behavior of d_{ij} on the (210) face. Here, from $V(r)$ alone, plane 1 would feel an upward force, plane 2 approximately no net force, plane 3 an upward force, and plane 4 a downward force. (See Table V to deduce these properties.) This would lead to a large d_{12}, small d_{23}, and large d_{34}. Except for d_{12} being below the bulk value [caused by $F(\rho)$], this type of behavior is predicted by JO and observed experimentally. However, potential 3 has a smaller d_{12} than JO, and a much larger d_{23} thanks to the stronger variations induced by the embedding function.

The d_{ij} properties of the other potentials can also be usually understood in terms of the competing influences of $F(\rho)$ and $V(r)$. Potential 1 has d_{ij}'s that can be largely understood in terms of nearest-neighbor repulsion and absence of second-neighbor attraction (actually the force is still slightly repulsive here). In the case of d_{23} for (111), the large downward force on plane 2 would be absent. In fact, it would be upward. So the large decrease in d_{23} seen in JO does not occur for potential 1. In fact, there is a large increase. Whereas the comparison between the EAM potentials and experiment certainly point to the desirability of significant nearest-neighbor repulsion in $V(r)$, as previously suggested by Johnson,[18] the d_{23} data point for (111) also indicates an important role for second-nearest-neighbor attraction as plane 3 of (111) has three fewer second neighbors than plane 2. Of course, at least some second-neighbor attraction seems necessary for bcc stability as evidenced by this common property of all the $V(r)$'s except potential 1, which yields only a metastable bcc phase. Moreover, the small value of d_{23} on (111), coupled with the large d_{34} value on (210), imply important roles of the second-neighbor attraction and first-neighbor repulsion, respectively.

As for parallel relaxation, JO gives the best fit with potential 3 almost as good. Potential 4, which has its minimum very close to the nearest-neighbor distance, significantly underestimates a_{12} on the (210) and (310) faces. Potential 1 gives very good (210) and (310) results.

For the a_{ij} the most significant deviations from bulk values occur for a_{12}, both experimentally and theoretically. Depending on the symmetry of neighbor atoms projected on the x-y plane, a_{12} is the difference in x (or y) coordinate between an atom on plane 1 and a nearest neighbor [second-nearest neighbor for (211)] on plane 2.[15] As with d_{12}, there is a competition between the influence of the embedding function to push atoms in the direction of the electron density gradient and the influence of repulsive or attractive two-body forces produced by missing neighbors. The electron density gradient is mainly in the z direction, so its influence on a_{12} should be less than on d_{12}. On all three surfaces [(210), (310), and (211)] the missing nearest-neighbor atoms are arranged such that the electron density gradient is toward the nearest neighbor in the second plane; i.e., this tends toward decreasing

a_{12} on (210), and (310) and increasing a_{12} on (211). Actually, for (210) and (310) there are two missing nearest-neighbor atoms on both sides of the surface atom with respect to the direction of asymmetry, but the net electron density gradient is toward decreasing a_{12}, with the (missing) atoms on the opposite side (however at larger z) tempering this effect somewhat. On (211) only one (higher) nearest neighbor tempers this effect. The situation of these nearest-neighbor atoms means that $V(r)$ will exert the opposite effect to that of $F(\rho)$ on a_{12}: surface atoms will be attracted toward these atoms because of the missing repulsion [if $V(r)$ is repulsive at this distance], tending to increase a_{12} on (210) and (310), decrease a_{12} on (211). The missing second neighbors are situated in such a way, for all faces, as to reinforce the influence of the nearest-neighbor two-body forces if $V(r)$ is attractive at the second-neighbor distance.

Potentials 3 and JO give rather good fits to the experimental data for a_{ij}. The fact that potential 1 gives very good results for (210) and (310) makes a case for first-neighbor repulsion being necessary and sufficient to fit a_{ij}, but of course we need some second-neighbor attraction for bulk bcc stability. Potentials where first-neighbor repulsion is largely absent in $V(r)$ do not predict satisfactory a_{ij} results. To a larger degree than d_{ij}, the a_{ij} reflects differences in $V(r)$ between different models because the influence of the embedding function is less. In fact, whereas the presence of an embedding function greatly decreases d_{12} from the bulk value, its presence does not have a large effect on a_{12} as changes from the bulk value are usually in the direction determined determined by $V(r)$ alone. Changes from the bulk value of a_{12} are larger on (211) because of the reduced tempering effect of the atom placement mentioned above.

Finally, we see from the results of this section how various features of the EAM produce certain surface-relaxation predictions, both perpendicular and parallel to the exposed face. For example, $F(\rho)$ has a large effect on the contraction of the first two planes, and also tends, to a lesser extent, toward an expansion of the distance between planes 2 and 3. Beyond this, by examining the number of missing neighbors as in Table V, we can assess, at least qualitatively, the effects of the two-body potential, with downward forces coming from missing attractive forces, and upward forces coming from missing repulsion. By looking at the downward and upward forces produced in this way by $F(\rho)$ and $V(r)$ we can get a good idea what the surface-relaxation results of a particular EAM would look like. Conversely, we can use these simple rules to adjust the features of the particular EAM to the surface-relaxation data. In the present study, for example, we have seen that the d_{23} on the (111) face points to a non-negligible amount of second-neighbor attraction in $V(r)$, while most of the rest of the data, especially d_{34} on (210) and a_{12} on all faces, indicate significant first-neighbor repulsion. This type of analysis is general and applies to fcc metals as well. Therefore surface-relaxation measurements, over several faces and down to several atomic planes in depth, can yield valuable information on EAM potentials in general.

V. CONCLUSIONS

In this work we have computed the perpendicular and parallel surface-relaxation properties of several different EAM models for bcc iron, and described how the features of these models influence surface-relaxation predictions. A surprisingly large variation in potential shapes occurs among EAM models, all consistent with the elastic bulk data and phonon spectra. There is at least one indication that our fitting procedure of insisting on an *exact* fit to certain points on the dispersion curves may not be the best method for iron: Potential I, produced in this manner, is stable with respect to bcc$\rightarrow$fcc transformation, but yields a noncubic bulk phase of lower energy than bcc. Also, the computed phonon spectra of potentials which were not explicitly fit to particular phonon frequencies, nevertheless showed good agreement with the measured spectra over the full range of frequencies. This indicates that explicit use of the phonon frequencies, necessary with some elements,[20] is not required for iron.

Most of the models at least reproduce some of the experimental features for surface relaxation, and a few give rather good quantitative fits. Nevertheless, there is quite a wide variation between different particular models. Therefore we conclude that merely fitting an EAM potential to bulk data does not in itself guarantee good surface results. However, this result does not invalidate the EAM approach at surfaces; some particular EAM potentials did give good results at surfaces. Thus surface relaxation may be regarded as an important testing ground for EAM interactions. If one wants to use a potential in a surface MD calculation, for example, the potential should be first tested for yielding satisfactory surface-relaxation predictions.

Alternatively, we could recommend the inclusion of surface-relaxation quantities in the database used to construct EAM potentials. One could use the d_{ij} and a_{ij} in fitting such potentials, and the discussion of Sec. III indicates how one could assess these quantities to determine at least the qualitative features of the desired EAM potential.

In bcc iron, potentials that have both significant first-neighbor repulsion and second-neighbor attraction in the equilibrium bulk give good fits to the surface-relaxation data. In the present study, potentials 3 and JO have these features and gave good (but not perfect) fits. In bcc iron, large deviations from terminated bulk structure occur in both perpendicular and parallel relaxation, even where the third or fourth atomic plane is involved. These potentials predicted most of the large deviations. In contrast to most of the other models, potentials 3 and JO have $V(r)$ qualitatively close to the Morse shape. It is comforting to see a Morse-like effective two-body potential being favored by a combination of bulk and surface data, since this shape has been suggested as a universal shape for interatomic forces, especially in metallic systems.[31] Interestingly, requiring a reasonable bulk thermal-expansion coefficient[24] also generally favors potentials of this shape for iron. However, the best potential with respect to the thermal expansion, potential 4, deviates somewhat from this shape and does not give as

good surface-relaxation results as potential 3 or JO. Nevertheless, a reasonable thermal-expansion coefficient is an important constraint and, at least in iron, seems to rule out potentials that coincidentally either yield poor surface results (potentials 2, 5, and 6) or yield anomalous stable bulk phases (potential 1).

We believe that this paper indicates a success of the EAM in the surface environment, at least for bcc iron. While the EAM can describe surface atomic structure, it nevertheless has to be used with care since, as we have shown, some (if not most) particular EAM interactions do not predict the correct surface relaxation. Therefore surface relaxation provides a very important test of EAM models from which we can learn much about the potential. Data from several faces extending at least a few atomic planes in depth would be necessary to gain such knowledge in general.

ACKNOWLEDGMENTS

We thank Dr. Mervine Rosen, Dr. George Mueller, and Dr. Gary Herling for many helpful discussions.

---

*Present address: Mail Zone 436-20-29, Land Systems Division, General Dynamics, P.O. Box 2074, Warren, MI 48090-2074.

[1]M. S. Daw and M. I. Baskes, Phys. Rev. Lett. **50**, 1285 (1983); Phys. Rev. B **29**, 6443 (1984).

[2]M. W. Finnis and J. E. Sinclair, Philos. Mag. A **50**, 45 (1984).

[3]S. M. Foiles, M. I. Baskes, and M. S. Daw, Phys. Rev. B **33**, 7983 (1986).

[4]R. A. Johnson, Phys. Rev. B **37**, 3924 (1988); D. J. Oh and R. A. Johnson, J. Mater. Res. **3**, 471 (1988).

[5]P. Hohenberg and W. Kohn, Phys. Rev. **136**, 864 (1964); M. J. Stott and E. Zaremba, Phys. Rev. B **22**, 1564 (1980).

[6]F. Ercolessi, E. Tosatti, and M. Parrinello, Phys. Rev. Lett. **57**, 719 (1986).

[7]Brian W. Dodson, Phys. Rev. B **35**, 880 (1986).

[8]Murray S. Daw, Surf. Sci. **166**, L161 (1986).

[9]S. M. Foiles, Surf. Sci. **191**, L779 (1987).

[10]M. A. Van Hove *et al.*, Surf. Sci. **103**, 189 (1981); **103**, 218 (1981); K. H. Rieder, T. Engel, R. H. Swendsen, and M. Manninen, *ibid.* **127**, 223 (1983); G. K. Binnig, H. Rohrer, Ch. Gerber, and E. Stoll, *ibid.* **144**, 321 (1984).

[11]P. Fenter and T. Gustafsson, Phys. Rev. **38**, 10 197 (1988), and references therein.

[12]D. L. Adams, H. B. Nielsen, and M. A. Van Hove, Phys. Rev. **20**, 4789 (1979); J. A. Davies, T. E. Jackman, D. P. Jackson, and P. R. Norton, Surf. Sci. **109**, 20 (1981). The relaxation measurements of Davies *et al.* are for metastable "almost clean" Pt(100) at 175K. The most stable structure for clean Pt(100) is a reconstructed 5×20 surface [M. A. Van Hove *et al.*, Surf. Sci. **103**, 218 (1981); T. A. Clarke, R. Mason, and M. Tescari, *ibid.* **40**, 1 (1973)].

[13]K. O. Legg, F. Jona, D. W. Jepsen, and P. M. Marcus, J. Phys. C **10**, 937 (1977).

[14]H. D. Shih, F. Jona, U. Bardi, and P. M. Marcus, J. Phys. C **13**, 3801 (1980).

[15]J. Sokolov, F. Jona, and P. M. Marcus, Phys. Rev. B **29**, 5402 (1984); **31**, 1929 (1985); Solid State Commun. **49**, 307 (1984); J. Sokolov, H. D. Shih, U. Bardi, F. Jona, and P. M. Marcus, J. Phys. C **17**, 371 (1984).

[16]H. D. Shih, F. Jona, D. W Jepsen, and P. M. Marcus, Surf. Sci. **104**, 39 (1981); J. Sokolov, F. Jona, and P. M. Marcus, Bull. Am. Phys. Soc. **30**, 459 (1985).

[17]W. Bendick and W. Pepperhoff, Acta. Metall. **30**, 679 (1982); Genrich L. Krasko and G. B. Olson, Phys. Rev. B **40**, 11 536 (1989).

[18]R. A. Johnson, Surf. Sci. **151**, 311 (1985); A. Machova and R. Mach, *ibid.* **211/212**, 125 (1989).

[19]P. Jiang, P. M. Marcus, and F. Jona, Solid State Commun. **59**, 275 (1986).

[20]J. M. Eirdon and S. Rao, Philos. Mag. Lett. **59**, 31 (1989).

[21]R. A. Johnson and D. J. Oh, J. Mater. Res. **4**, 1195 (1989).

[22]S. M. Foiles, Phys. Rev. B **32**, 7685 (1985).

[23]M. Baskes, Phys. Rev. Lett. **59**, 2666 (1987).

[24]S. M. Foiles and M. S. Daw, Phys. Rev. B **38**, 12 643 (1988).

[25]J. H. Rose, J. R. Smith, F. Guinea, and J. Ferrante, Phys. Rev. B **29**, 2963 (1984).

[26]B. N. Brockhouse, H. Abou-Helal, and E. D. Hallman, Solid State Commun. **5**, 211 (1967).

[27]V. J. Minkiewicz, G. Shirane, and R. Nathans, Phys. Rev. **162**, 528 (1967).

[28]This value of E_{v1}^{UF} was taken from Table I of Ref. 21, which refers to K. Furderer *et al.*, in *Vacancies and Interstitials in Metals and Alloys,* edited by C. Abromeit and H. Wollenberger (Trans. Tech, Aedermannsdorf, Switzerland, 1987), p. 125; and L. De Schepper *et al.*, *ibid.*, p. 131.

[29]D. Fincham and D. M. Heyes, Adv. Chem. Phys. **63**, 493 (1985).

[30]*Numerical Recipes* edited by William H. Press, Brian P. Flannery, Saul A. Teukolsky, and William T. Vetterling (Cambridge University Press, Cambridge, England, 1988), pp. 301–307.

[31]G. C. Abell, Phys. Rev. B **31**, 6184 (1984); James H. Rose, John R. Smith, and John Farrante, *ibid.* **28**, 1835 (1983); J. Tersoff, Phys. Rev. Lett. **56**, 632 (1986).